

An Adaptive Radial Basis Function Neural Network Filter for Noise Reduction in Biomedical Recordings

J. Mateo-Sotos¹ · A. M. Torres¹ ·
E. V. Sánchez-Morla^{2,3} · J. L. Santos⁴

Received: 25 February 2015 / Revised: 8 February 2016 / Accepted: 9 February 2016 /

Published online: 1 March 2016

© Springer Science+Business Media New York 2016

Abstract Electroencephalogram (EEG) recordings often experience interference by different kinds of noise, including white, muscle and baseline, severely limiting its utility. Artificial neural networks (ANNs) are effective and powerful tools for removing interference from EEGs. Several methods have been developed, but ANNs appear to be the most effective for reducing muscle and baseline contamination, especially when the contamination is greater in amplitude than the brain signal. An ANN as a filter for EEG recordings is proposed in this paper, developing a novel framework for investigating and comparing the relative performance of an ANN incorporating real EEG recordings. This method is based on a higher-order statistics-based radial basis function (RBF) network. This ANN improves the results obtained with the conventional EEG filtering techniques: wavelet, singular value decomposition, principal component analysis, adaptive filtering and independent components analysis. Average results for the RBF-based method provided a noise reduction (SIR) of (mean± SD) SIR = 19.3 ± 0.3 in contrast to traditional compared methods that, for the best case,

✉ J. Mateo-Sotos
jsOTOS7823@gmail.com

A. M. Torres
anatorres2342@gmail.com

E. V. Sánchez-Morla
emasanchez@sescam.jccm.es

J. L. Santos
jlsantos@sescam.jccm.es

¹ Polytechnic School, University of Castilla-La Mancha, Cuenca, Spain

² Department of Psychiatry, Hospital Universitario de Guadalajara, 19002 Guadalajara, Spain

³ School of Medicine, Alcalá University, Madrid, Spain

⁴ Department of Psychiatry, Virgen de la Luz Hospital, Cuenca, Spain

yielded $SIR = 15.2 \pm 0.3$. The system has been evaluated within a wide range of EEG signals. The present study introduces a new method of reducing all EEG interference signals in one step with low EEG distortion and high noise reduction.

Keywords Radial basis function · Neural network · Adaptive filter · Noise

1 Introduction

Noise reduction is a matter of considerable importance in biomedical signal processing applications, especially electroencephalogram (EEG) analysis [46]. The EEG signal can be distorted by many sources of unwanted electrical activity, called artefact sources. Some artefacts are readily distinguished, others so closely resemble cerebral activity that their interpretation is taxing even to the most experienced electroencephalographer. Low-frequency (0–4 Hz) and high-frequency (more 20 Hz) bands of EEG may pick up artefacts, such as eye movements and muscle activity, and therefore should be evaluated with caution. One useful categorization of artefacts is based on their origin: physiological (from patient's own generator sources, e.g. movements, muscle (EMG) activity or rigidity, head and body motion, sustained eye movements, cardiogenic, sweat and baseline noise) or technical (extraphysiological, externally generated), such as environmental interference caused by 50 or 60 Hz power supply lines, radiation from lights, improper sensor placement, unusual or excessive electrical interference and radio frequency emissions from nearby medical devices. This categorization is also applicable to other bioelectrical signals. While the influence of technical artefacts can be reduced, to a large degree, by paying extra attention to the attachment of electrodes to the body surface, it is impossible to avoid the influence of physiological artefacts. Accordingly, a majority of algorithms developed for EEG artefact processing are intended to reduce physiological interferences in order to get accurate information about the brain activity and avoid mistakes in its interpretation [46].

Regarding muscle and baseline noise, several methods have been suggested for their reduction. These signal processing techniques used for noise elimination include band-pass filtering, fast Fourier transform, autocorrelation, autoregressive modelling and time-varying frequency estimation method [13, 29, 30, 44, 46]. Other authors implement Kalman filtering [3, 49], Hammerstein filtering (HF) [12, 19] and nonlinear Bayesian filtering [39, 40]. Singular value decomposition (SVD) [28, 36, 50] has also been applied in order to reduce noise in biomedical signals. One of the common approaches is the adaptive filtering (AF) architecture which has been used for interference cancellation of EEG [7, 32, 41, 48, 51] and wavelet [6, 9, 45, 52]. In this context, principal component analysis (PCA) [10, 11, 22, 47] and independent component analysis (ICA) [1, 15, 23, 26, 31, 38] have become popular for analysing biomedical data (e.g. EEG and EMG). One of the main advantages of these approaches relates to their applicability to multisensory observations of mixed signals. However, PCA is unable to separate some artefact signals from brain signals when they have similar amplitudes [22]. In addition, both PCA and SVD perform well only if the noise level is low enough and a signal subspace and noise subspace are orthogonal to each other.

For practical applications, the orthogonality requirement is usually not valid. On the other hand, ICA cannot guarantee that some individual independent components (ICs) contain only noise and not information about useful sources, especially in biomedical applications. Thus, the problem of detection and filtering the “useful” part of each IC is still open, and additional tools are needed to solve it.

Artificial neural networks (ANNs) are a kind of powerful methods that have been applied to many areas with success such as adaptive control, pattern classification and medical research [2, 8, 17, 18, 33, 42, 53, 54]. In this paper, a new noise cancellation method based on a radial basis function (RBF) neural network and higher-order statistics [5, 25, 27, 34] is proposed. The system can be applied to both single- and multi-lead EEG recordings. The proposed RBF network has been developed like a hierarchically layered structure. It starts with a small number of RBFs and then adds new RBFs if the approximation error is larger than some predetermined threshold, and there is no existing RBF that can efficiently represent the current input. The RBF has been also chosen mainly because of its adaptability to the nonlinear and time-varying features of the noise. Computer experiments have demonstrated that the developed algorithm can improve the noise reduction over the compared systems. Furthermore, the results have shown that this new method can maintain the original shape of the EEG signal in very low SNR conditions in which the brain signal is mixed with the noise. Several important advantages have been obtained with this system. Firstly, different noise types have been reduced simultaneously, a low distortion of the signal has been caused, and finally, clinical information has been maintained. Besides, this system could be applied to a wide range of biomedical signals.

The paper is organized as follows: Sect. 2 introduces the materials used in this study. Section 3 presents our proposed approach. The description of the experiments and the discussion of the results are given in Sects. 4 and 5, respectively. Finally, the conclusions of this paper are summarized in Sect. 6.

2 Materials

In this section, the characteristics of the real clinical signals and the synthesized signals used for this work are presented. The database generated in this paper was created from Psychiatric and Neurophysiology departments in the hospital Virgen de la Luz in Cuenca (Spain). Eighty healthy subjects (43 males, 37 females, 36 adults with an average 31 years old, 32 youth with an average 22 years old and 12 children with an average 14 years old) were selected. The electrodes were placed according to the International 10–20 System, and EEG data were recorded at 250 Hz using Brain Vision with 32 channels and Viasys Healthcare—NicoletOne equipment with 16 channels. The vertical EOG (VEOG) signal was recorded from the right eye (2.5 cm below and above the eyeball); the horizontal EOG (HEOG) signal was recorded from the outer canthus, and reference was located on A2 (right earlobe). On the other hand, several sleep studies were also included. These signals offered different noises such as power-line interference, artefacts, baseline and muscle noise. All signals obtained from the hospital were classified into three groups, each having a different function within the filtering process. The first group comprised (45 %) of the signals randomly

selected, which were employed to network training. The second group (25 %) helped to validate the proper ANN working. Finally, the third group (30 %) was used to compare the ANN proposed system with other previously proposed systems deeply accepted by the scientific community.

The synthesized recordings were comprised of 100 signals that lasted 30–60 min. Also, several sleep testings of approximately 8 h, were included in this study, and if the hospital recording was noisy, it was filtered to remove its noise [46]. Once this process was completed, baseline and muscle noise were sequentially added to the EEG signal as defined by Eq. 1 [46], where $d(t)$ is the EEG recording, A is the amplitude of the added noise and $n_s(t)$ is the noise signal. Muscle noise is coloured noise and affects the entire frequency range of EEG; however, baseline noise is characterized by low frequency. A and $n_s(t)$ were two independent continuous random variables. The main aim was to estimate the clean signal $d(t)$ from the noisy signal $x(t)$. In order to have each signal with one different noise, the noise added to each signal was generated randomly and each signal had a different noise added by a different noise realization. Although there are different ways of generating coloured noise, the method reported by Sameni et al. [40] was chosen. The signal colour was modelled by a single parameter which represents the slope of a spectral density function which decreases monotonically with frequency $S(f) \propto \frac{1}{f^\beta}$, where f is the frequency and β is the measure of noise colour. Depending on the chosen β , different types of noise can be generated: white noise ($\beta = 0$); pink noise ($\beta = 1$) or flicker noise; and brown noise ($\beta = 2$).

$$x(t) = d(t) + An_s(t). \quad (1)$$

The amplitude was changed to achieve signals under SNR variation that ranged between -5 and 30 dB. Regarding muscle and baseline noise, different portions of noise were chosen from hospital recordings. Once the signal was separated, it was also added to the $d(t)$ signal in order to modify the SNR range from -5 to 30 dB. In order to have each signal with one different noise, the noise added to each signal was generated randomly and each signal had a different noise added by a different noise realization.

The third group of signals was made up of 30 % signals, and neither noise nor variation was added or modified (real signals). These signals were also used to compare the above-mentioned methods to ANN.

3 Method

ANNs are a type of nonlinear processing system ideally suited to a wide range of tasks, especially those in which there is no existing algorithm for task completion. ANNs can be trained to solve certain problems using a learning method and sample data [17, 18]. In this way, identically constructed ANN can be used to perform different tasks based on the training received. With proper training, ANNs are capable of generalization, the recognition of similarities among different input patterns, especially patterns corrupted by noise [17]. Training is the development of increasing networks in which nodes are systematically added in the hidden layer during the learning process [14, 18, 21].

3.1 Proposed System

RBF neural networks are function approximation models that can be trained by means of examples to implement a desired input–output mapping [4,8]. In fact, RBF models are closely related to function approximation models used to perform interpolation [8]. Under certain mild conditions, RBF neural networks are capable of approximating arbitrarily well any function [8]. The performance of a RBF depends on the number and centres of the radial basis functions, their shapes, and the method used for learning the input–output mapping. The centres of the RBF are often determined by the k -means clustering algorithm [8,20].

The proposed RBF network in the present work has a hierarchically layered structure. It starts with a small number of RBFs and then adds new RBFs if the approximation error is larger than some predetermined threshold, and there is no existing RBF that can efficiently represent the current input. Moreover, some of the existing RBFs can be removed if the approximation error is small and other conditions still are satisfied [24]. In this study, different types of RBFs have been employed to develop the proposed noise cancellation. The implementations using Gaussian RBF (GRBF) and raised-cosine RBF (RCRBF) are discussed and compared. Although the GRBF network possesses the property of universal approximation, the network’s training and output evaluation are still time-consuming. This is because the GRBF has the unbounded support and thus each RBF has nonzero output over the whole input space. On the other hand, the RCRBF is proposed because of its compact support [42]. The property of compact support enables much faster network training and output evaluation as the complexity of the network and the dimensionality of the input space increase [27].

The proposed RBF network structure is shown in Fig. 1. Let the input signal $x(t)$ be

$$x(t) = d(t) + n_s(t), \quad (2)$$

where $d(t)$ and $n_s(t)$ represent the clean signal and noise signal at the iteration t , respectively. Based on the scheme of adaptive line enhancement (ALE) [16], the delayed version of $x(t)$ can be used as the reference signal $p(t)$ and is given by

$$p(t) = x(t - \Delta). \quad (3)$$

Here, the prediction depth Δ is usually selected by the unit of sampling period. Let N_0 and N_1 denote the number of the input and hidden nodes, respectively; the estimate $\hat{d}(t)$ of $d(t)$ can be defined by

$$\hat{d}(t) = \xi(t)^T w(t), \quad (4)$$

where $\xi(t) = [\xi_1(t), \xi_2(t), \dots, \xi_{N_1}(t)]^T$ represents the output vector of the hidden nodes, generated by radial basis function, and $w(t) = [w_1(t), w_2(t), \dots, w_{N_1}(t)]^T$ denotes the weight vector connecting the hidden nodes with the output node.

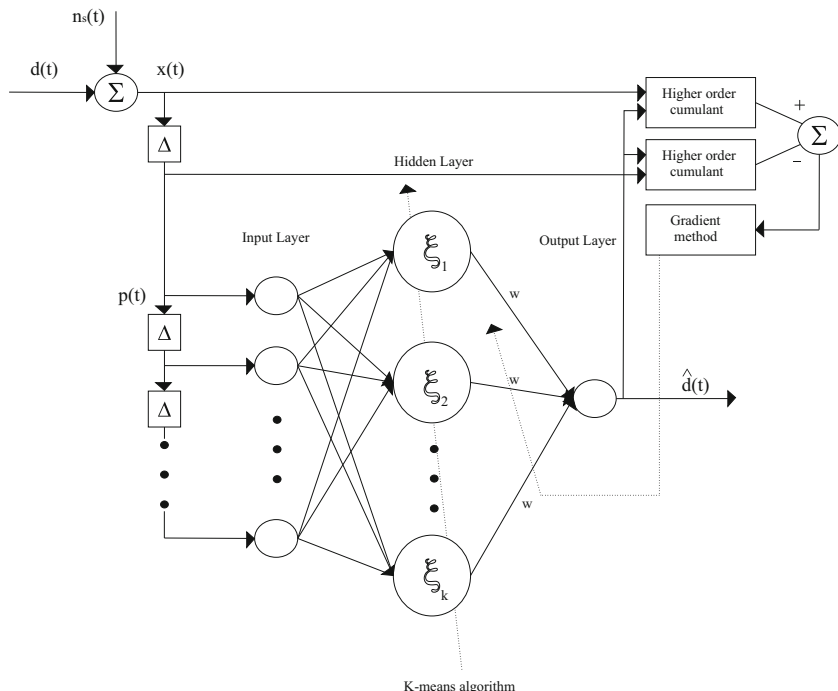


Fig. 1 Proposed scheme of higher-order statistics-based RBF network for noise cancellation

Regarding the two aforesaid different implementations of RBFs (Fig. 2), the GRBF is characterized by the following activation function

$$\xi_k(t) = \exp\left(-\frac{(p(t) - c_k(t))^2}{2\sigma^2}\right), \quad (5)$$

whereas the RCRBF is a compact support RBF, which is given by

$$\xi_k(t) = \begin{cases} \frac{1}{2} \left(1 + \cos\left(\frac{\pi(p(t) - c_k(t))}{\sigma(t)}\right)\right) & \text{if } |p(t)| \leq \sigma(t) \\ 0 & \text{if } |p(t)| > \sigma(t) \end{cases}, \quad (6)$$

where $p(t) = [p(t), p(t-1), \dots, p(t-N_0+1)]^T$ is the vector of the input nodes and $c_k(t)$ the centre in the k th hidden node. In addition, $\sigma(t)$ represents the width of the centres and can be defined as the variance of the input vector. The centre $c_k(t)$ can be calculated by the k -means clustering algorithm [20], which is a self-organized learning procedure, and the weight vector $w(t)$ is commonly adapted by the normalized LMS algorithm [16].

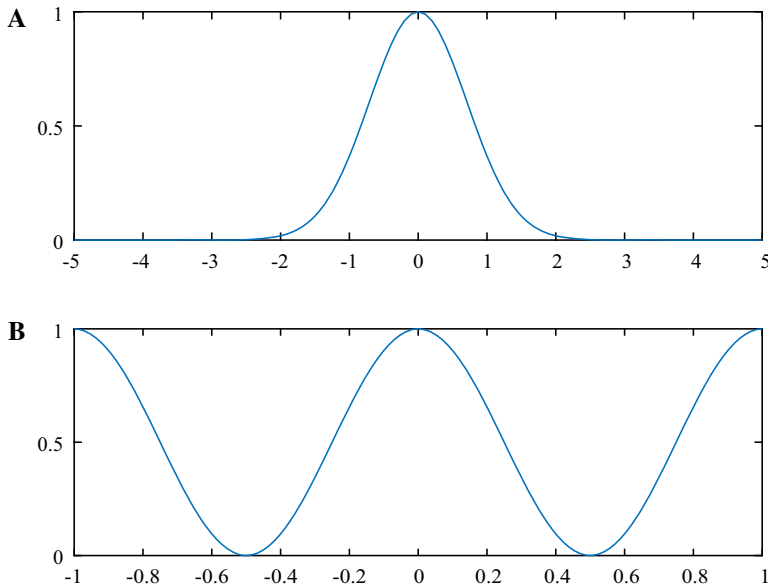


Fig. 2 Two different types of rbf used in the study, where **a** shows the gaussian function and **b** plots cosine radial basis function

The weight vector can be updated by

$$w(t+1) = w(t) + \frac{(1 + \xi^T(t)\xi(t))}{\xi}(t)(x(t) - \hat{d}(t)), \quad (7)$$

where α represents the learning rate ($\alpha = (1 + \xi^T(t)\xi(t))$), $\hat{d}(t)$ the estimate signal, $x(t)$ the input signal and $\xi(t)$ the activation function. Obviously, adapting weights is easily affected by additional noise $n_s(t)$ due to that $e(t)$ is correlated with additional noise $n_s(t)$, i.e. $e(t) = x(t) - \hat{d}(t) = d(t) + n_s(t) - \hat{d}(t)$.

The proposed scheme of higher-order statistics-based RBF network for signal enhancement is shown in Fig. 1 [5, 25, 27, 34]. Certain nonlinear combinations of moments and cumulants arise naturally when analysing sums of independent random variables. The n th moment of a real-valued random variable X with density $f(x)$ is

$$\mu_n = E(X^n) = \int_{-\infty}^{\infty} x^n f(x) dx, \quad (8)$$

for integer $n = 0, 1, \dots$. The value is assumed to be finite. Provided that it has a Taylor expansion about the origin, the moment generating function

$$M(\phi) = E(e^{\phi X}) = E(1 + \phi X + \dots + \phi^n X^n / n! + \dots), \quad (9)$$

$$M(\phi) = \sum_{r=0}^{\infty} \mu^n \phi^n / n!, \quad (10)$$

is an easy way to combine all of the moments into a single expression. The n th moment is the n th derivative of M at the origin [34,37,43].

The cumulants C_n are the coefficients in the Taylor expansion of the cumulant generating function about the origin [34,37,43]

$$K(\phi) = \log M(\phi) = \sum_n C_n \phi^n / n!. \quad (11)$$

For a set of real stationary variables $\{h_i(t)\}$, $i = 1, 2, 3, \dots$, the n th-order cross-cumulant of $\{h_i(t)\}$ can be represented as follows:

$$\begin{aligned} & C_{h_1 h_2 \dots h_n} (\tau_1, \tau_2, \dots, \tau_{n-1}) \\ & \equiv \text{Cum} [h_1(t), h_2(t + \tau_1), h_3(t + \tau_2), \dots, h_n(t + \tau_{n-1})]. \end{aligned} \quad (12)$$

Here, $\text{Cum}[\cdot]$ indicates the cumulant operator [5,27,34]. Under the assumption that the n th-order cumulants ($n > 2$) of the desired and reference signals exist, they can be expressed by

$$C_{xpp \dots p} (\tau_1, \tau_2, \dots, \tau_{n-1}) = \text{Cum} [x(t), p(t + \tau_1), p(t + \tau_2), \dots, p(t + \tau_{n-1})]. \quad (13)$$

Since $d(t)$ and $n_s(t)$ in the desired and reference signal are independent [34], Eq.(13) can then be simplified as

$$C_{xpp \dots p} (\tau_1, \tau_2, \dots, \tau_{n-1}) = \text{Cum} [d(t), d(t + \tau_1 - \Delta), \dots, d(t + \tau_{n-1} - \Delta)] \quad (14)$$

$$C_{xpp \dots p} (\tau_1, \tau_2, \dots, \tau_{n-1}) = C_{dd \dots d} (\tau_1 - \Delta, \tau_2 - \Delta, \dots, \tau_{n-1} - \Delta). \quad (15)$$

Similarly, the n th cumulant of the filtered output signal can also be given by

$$C_{\hat{d}pp \dots p} (\tau_1, \tau_2, \dots, \tau_{n-1}) = C_{\hat{d}dd \dots d} (\tau_1 - \Delta, \tau_2 - \Delta, \dots, \tau_{n-1} - \Delta). \quad (16)$$

From Eqs. (15) and (16), it is obvious that the influence of additional noise $n_s(t)$ on the learning algorithm of higher-order statistics-based RBF can be reduced effectively, due to that the difference between the higher-order cumulants of $x(t)$ and the filtered output $\hat{d}(t)$ is used as the learning criterion Ψ . And the learning criterion Ψ can then be defined by

$$\Psi = \sum_{\tau_1} \sum_{\tau_2} \dots \sum_{\tau_{n-1}} \frac{1}{2} \left[C_{\hat{d}pp \dots p} (\tau_1, \tau_2, \dots, \tau_{n-1}) - C_{xpp \dots p} (\tau_1, \tau_2, \dots, \tau_{n-1}) \right]^2$$

$$\begin{aligned}
&= \sum_{\tau_1} \sum_{\tau_2} \cdots \sum_{\tau_{n-1}} \frac{1}{2} [C_{\hat{d}dd...d}(\tau_1 - \Delta, \tau_2 - \Delta, \dots, \tau_{n-1} - \Delta) \\
&\quad - C_{dd...d}(\tau_1 - \Delta, \tau_2 - \Delta, \dots, \tau_{n-1} - \Delta)]^2 \\
&= \sum_{\tau_1} \sum_{\tau_2} \cdots \sum_{\tau_{n-1}} \frac{1}{2} \left[\sum_{j=1}^{N_1} w_j C_{\xi_j pp...p}(\tau_1, \tau_2, \dots, \tau_{n-1}) \right. \\
&\quad \left. - C_{xpp...p}(\tau_1, \tau_2, \dots, \tau_{n-1}) \right]^2. \tag{17}
\end{aligned}$$

Equation (17) can be expressed in a matrix form

$$\Psi = \frac{1}{2} [C_{\xi pp...p}w - C_{xpp...p}] [C_{\xi pp...p}w - C_{xpp...p}]^T, \tag{18}$$

where $C_{\xi pp...p}$ and $C_{xpp...p}$ are an $N_\Theta \times N_1$ matrix and an $N_\Theta \times 1$ column vector and N_Θ denotes the number of points in the set Θ . In order to minimize Ψ , the gradient descent method was applied. The gradient of Ψ is given by

$$\nabla w(t) = \frac{\partial \Psi}{\partial w(t)} = -C_{\xi pp...p}^T(t) [C_{xpp...p}(t) - C_{\xi pp...p}(t)w(t)]. \tag{19}$$

Consequently, the adaptation formula can be calculated by

$$w(t+1) = w(t) - \frac{\alpha}{(1 + tr(C_{\xi pp...p}^T C_{\xi pp...p}))} \nabla w(t), \tag{20}$$

where tr is the trace of the matrix. Under the assumption that $d(t)$ approximates to $\hat{d}(t)$, the learning criterion in Eq. (17) will be close to optimal. Therefore, by using the higher-order statistics-based learning algorithm, the influence of additional noises $n_s(t)$ on $C_{xpp...p}$ can be reduced and provide better performance.

3.2 Experimental Results

The performance of RCRBF neural networks was evaluated and compared with that of feedforward neural networks (FFNN) with sigmoid hidden units and conventional RBF neural networks with GRBF. Conventional radial basis function neural networks were trained by a hybrid learning scheme [8]. The centres of the RBF were determined according to an unsupervised procedure relying on the k -means algorithm. The widths of the GRBF were computed according to the nearest heuristic prototype [8]. The centres of the RBF were fixed during the supervised learning process. Radial basis function neural networks were trained by a fully supervised procedure based on gradient descent. This procedure involved the update of the output weights and the centres $\{c_k\}$ of the radial basis functions [8].

Table 1 Average number N of adaptation cycles required for training various RBF with c radial basis functions and FFNNs with n hidden units to noise cancellation and percentage of average error produced on the training set (E_{tr}) and the testing set (E_{ts})

Feed forward NNs				
n_h	20	25	30	35
N	202.3	215.1	219.3	221.5
$E_{tr}(\sigma_{tr})$	12.29 (1.31)	10.97 (1.09)	10.15 (1.28)	9.95 (1.07)
$E_{ts}(\sigma_{ts})$	13.18 (1.27)	12.31 (1.25)	11.46 (1.24)	10.97 (1.18)
Gaussian RBF NNs				
c	8	10	12	14
N	248.3	261.2	265.5	279.7
$E_{tr}(\sigma_{tr})$	8.97 (1.12)	8.51 (1.19)	8.02 (1.05)	7.49 (1.01)
$E_{ts}(\sigma_{ts})$	9.21 (1.18)	9.13 (1.23)	9.51 (1.17)	8.03 (1.08)
Cosine RBF				
c	8	10	12	14
N	206.2	218.5	224.8	229.7
$E_{tr}(\sigma_{tr})$	2.87 (0.73)	2.14 (0.55)	2.07 (0.54)	1.85 (0.42)
$E_{ts}(\sigma_{ts})$	2.99 (0.80)	2.20 (0.57)	2.08 (0.53)	1.97 (0.51)

The numbers in parentheses represent the standard deviation

The results of these experiments are summarized in Table 1, which shows the number of adaptation cycles required for training the neural networks mentioned above, and the percentage of errors produced on average by the trained neural networks on the training and testing sets. According to Table 1, RCRBF networks produced the smallest percentage of errors on both training and testing sets among all the RBF models tested in the experiments. The performance differences among RBF models became more significant as the number of RBFs decreased.

In applications where the goal is to create a system that generalizes well in unseen examples, the problem of over-training has emerged. This arises in over-complex or over-specified systems when the capacity of the network significantly exceeds the needed free parameters. In order to avoid this problem, cross-validation technique to check the presence of over-training and select optimal parameters in order to minimize the generalization error has been used. Cross-validation is a model assessment technique used to evaluate a machine learning algorithms performance in making predictions on new datasets that it has not been trained on. This is done by partitioning a dataset and using a subset to train the algorithm and the remaining data for testing. Because cross-validation does not use all of the data to build a model, it is a commonly used method to prevent overfitting during training [4]. Figure 3 shows the cross-correlation study for RCRBF, which has been selected because of its better adaptation to the problem. In this figure, an optimal point of training and why the proposed system has a correct predictive accuracy are obtained. If you increase the number of iterations from the “best” point, the result does not improve due to over-training.

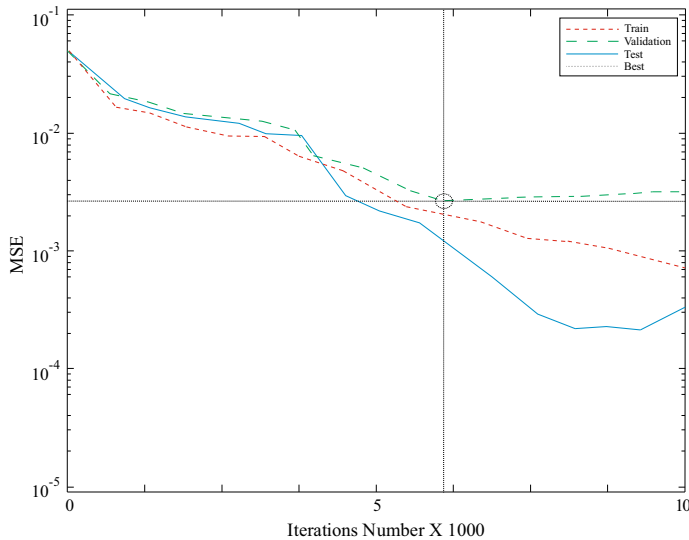


Fig. 3 Cross-correlation graph obtained for the RCRBF. The *small dashed line* shows the evolution of the MSE for the training phase; in this phase, the signals of group 1 have been used. The *large dashed line* shows the evolution of the MSE for the validation phase; in this phase, the signals of group 2 have been used. The *continuous line* shows the evolution of the MSE for the test phase; in this phase, the signals of group 3 have been used. The *circle* represents optimum point

3.3 Performance Assessment

The proposed method was thoroughly tested and compared with the previously published noise reduction techniques, using the quantitative measures of performance that will be next described.

The noise reduction was computed by comparing the estimated and the original EEG in terms of the cross-correlation (CC) and mean square error (MSE). The cross-correlation index measured the similarities between two signals and became 1 in the case of perfect matching and 0 in the case of completely different and unrelated signals

$$\text{CC} = E[\widehat{d}(t) \cdot d(t)], \quad (21)$$

where $E[\cdot]$ is the expectation operator of $\widehat{d}(t)$ and $d(t)$, respectively. On the other hand, the MSE was defined as

$$\text{MSE} = \sqrt{\sum (d(t) - \widehat{d}(t))^2}. \quad (22)$$

In order to analyse the effect of noise, the signal-to-interference ratio (SIR) was used. This parameter was defined as

$$\text{SIR} = 20 \log \left(\sqrt{\frac{E\{(x(t) - d(t))^2\}}{E\{(\widehat{d}(t) - d(t))^2\}}} \right), \quad (23)$$

where $x(t)$ is the input signal to the system, $\hat{d}(t)$ the output and $d(t)$ the original recording without noise. This parameter was used to evaluate both the output signals and the distortion.

To reinforce the validation of results, the SNR improvements (SNRIs) were used, because it has been widely accepted in the community [40, 51]. The SNRI was defined as the output SNR of the filter (in decibels) minus the input SNR (in decibels); hence, we defined the SNR as

$$\text{SNR} = 10 \cdot \log 10 \left(\frac{|P_{\text{signal}}|}{|P_{\text{noise}}|} \right), \quad (24)$$

where the factor P_{noise} was defined as the power of $n_s(t)$, where $n_s(t) = x(t) - d(t)$. For synthetic signals, this value was calculated directly by knowing the noise signal $n_s(t)$ and, for real signals, $n_s(t) = x(t) - d(t)$. In this moment, it was possible to define the SNRI as

$$\text{SNRI}(dB) = \text{SNR}_{\text{out}}(dB) - \text{SNR}_{\text{in}}(dB). \quad (25)$$

Negative SNRI indicated apparently a degradation of the SNR input which, eventually, was caused by the filtering procedure.

4 Results

Extensive experiments were carried out to evaluate the performance of the proposed method, and its performance was compared with several systems based on wavelet, SVD, PCA, AF, HF and ICA in order to reduce muscle and baseline noise.

4.1 Muscle Noise

In order to research the analysis of the muscle noise, three parameters were calculated: CC, SIR and SNRI.

The proposed method was able to improve the results with respect to the other systems, as given in Table 2. The table shows average values \pm SD. As can be observed, the RBF is able to reach the closest result to 1 in CC. Furthermore, the SIR value achieved by the wavelet, SVD, PCA, AF, HF and ICA methods is lower than the RBF. Therefore, the proposed system outperforms the results obtained by the other methods. Spectral correlation has been calculated by using 8192 points within FFT.

Figure 4 shows the results obtained with wavelet, SVD, PCA, AF, HF, ICA and the RBF using an input SNR of 8 dB. As can be appreciated, our RBF method followed the original signal very precisely. On the other hand, the ICA method overcomes HF and AF systems. Despite all, these last methods contain some large waves which do not appear in the original EEG.

Figure 5 shows the SNRI and its standard deviation (SD). The wavelet, SVD, PCA, AF and HF methods degraded SNR inputs of less than 10 dB, whereas the RBF kept

Table 2 Average values of CC (temporal and spectral) and SIR obtained with wavelet, SVD, PCA, AF, HD, ICA and RBF for muscle noise

Methods	CC (time)	CC (spectral)	SIR
Wavelet	0.85 ± 0.03	0.86 ± 0.03	12.7 ± 0.3
SVD	0.88 ± 0.04	0.89 ± 0.03	13.5 ± 0.4
PCA	0.82 ± 0.04	0.84 ± 0.03	12.4 ± 0.5
AF	0.90 ± 0.02	0.91 ± 0.02	14.8 ± 0.3
HF	0.91 ± 0.02	0.92 ± 0.03	15.0 ± 0.3
ICA	0.92 ± 0.02	0.93 ± 0.02	15.2 ± 0.3
RBF	0.97 ± 0.02	0.98 ± 0.02	19.3 ± 0.3

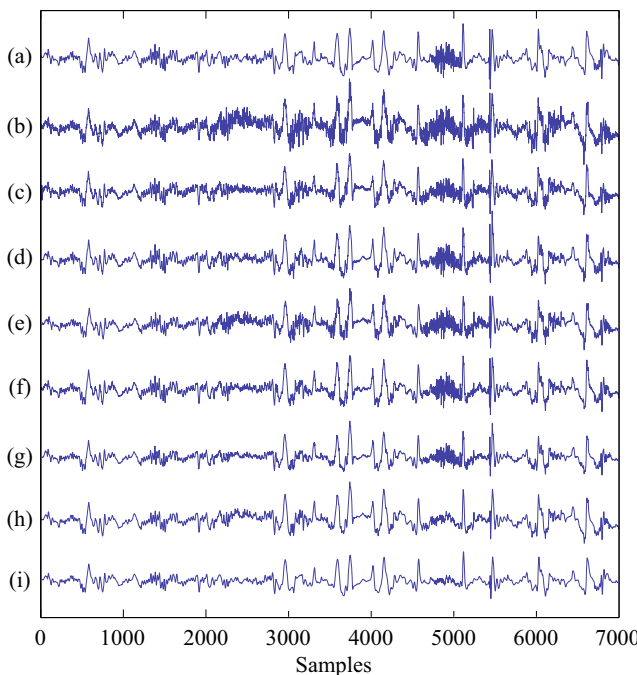


Fig. 4 Comparison of the muscle noise removal by proposed system and traditional techniques for F7-T3 derivation. *a* Original recording without processing. *b* Input signal of 8 dB muscle noise used to compare the different methods. *c* Filtering results for muscle noise with the wavelet method. *d* Filtering results for muscle noise with the SVD method. *e* Filtering results for muscle noise with the PCA method. *f* Filtering results for muscle noise with the AF method. *g* Filtering results for muscle noise with the HF method. *h* Filtering results for muscle noise with the ICA method. *i* Filtering results for muscle noise with the RBF

this value positive until 25 dB and avoided a degradation of the SNR input. When the input SNR was 30 dB, the biggest difference was achieved with RBF method.

Concerning the conventional filtering methods, the ICA method overcame both the SVD and PCA. According to these plots, SD was proving that ICA outperformed the other traditional methods, but, at the same time, the least deviation of all was obtained

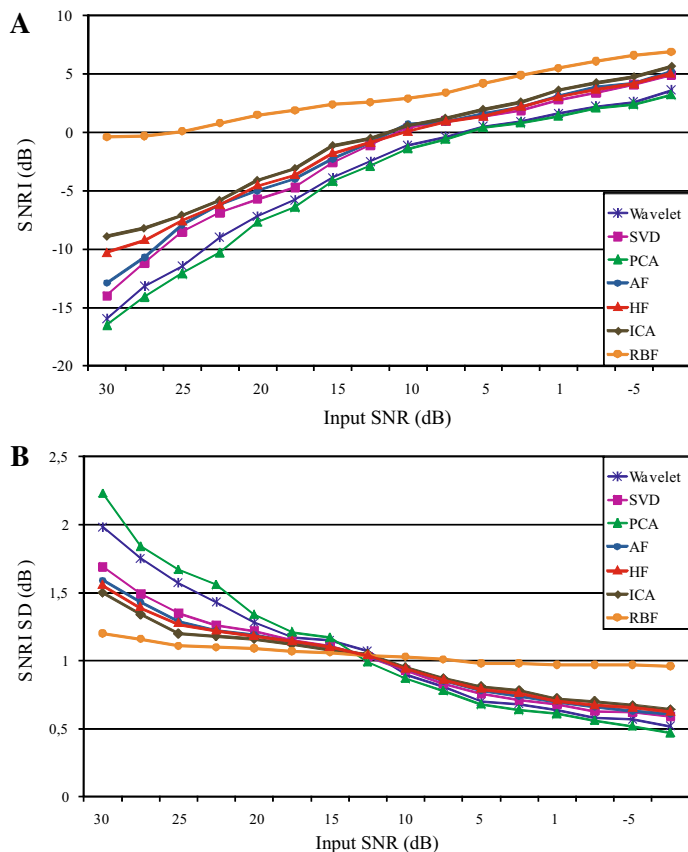


Fig. 5 Results for the study of the muscle noise reduction, where **a** shows the mean filter output SNRI versus different input SNRs and **b** plots SD of the filter output SNRI versus different input SNRs

with our RBF. Thus, the RBF results were the most robust compared with other dataset variations as given in Table 2 and Fig. 5.

4.2 Baseline Noise

The performance of RBF with baseline noise was also compared to the standard filtering techniques wavelet, SVD, PCA, AF, HF and ICA. The CC and SIR parameters with different SNRs with a baseline frequency between 0.1 and 0.6 Hz are given in Table 3. The table shows average values \pm SD. As can be observed, RBF outperforms traditional systems. Only the ICA method is positioned close to the RBF values, and notably, the least effective performance was achieved with the HF, AF, PCA, SVD and wavelet methods.

Table 4 presents the average results for MSE. The table shows average values \pm SD. As can be seen, when the baseline frequency was < 0.2 Hz, the results of the ICA method were suitable, while the RBF fulfilled the filtering process when the baseline

Table 3 Average values of CC (temporal and spectral) and SIR obtained with wavelet, SVD, PCA, AF, HF, ICA and RBF for baseline noise

Methods	CC (time)	CC (spectral)	SIR
Wavelet	0.86 ± 0.03	0.87 ± 0.03	13.2 ± 0.3
SVD	0.90 ± 0.03	0.91 ± 0.03	14.3 ± 0.3
PCA	0.85 ± 0.04	0.86 ± 0.04	12.6 ± 0.3
AF	0.91 ± 0.03	0.92 ± 0.03	15.1 ± 0.2
HF	0.92 ± 0.03	0.93 ± 0.03	15.3 ± 0.2
ICA	0.93 ± 0.02	0.94 ± 0.02	15.4 ± 0.2
RBF	0.97 ± 0.02	0.98 ± 0.02	19.7 ± 0.2

frequency was <0.6 Hz. On the other hand, when the SNR was -2.7 dB, the MSE [Eq. (22)] was 3.6 %. The aim was to find the best result between information preservation and baseline wander removal. This distortion affected neither pulse diagnosis efficiency nor pulse pattern recognition. The frequency content of the EEG baseline noise was rich, but the baseline noise was completely removed by the RBF method without reducing the clinical signal information.

In Fig. 6, the results for baseline noise removal yielded by wavelet, PCA, SVD, AF, HF, ICA and the proposed RBF are represented making use of a synthesized noisy signal with 8 dB of SNR. As can be observed, the RBF strategy was able to follow the original signal very precisely. On the other hand, the ICA method overcame HF, wavelet, PCA and SVD systems. Despite all, these last methods contained some waves which did not appear in the original EEG.

EEG techniques such as low-resolution electromagnetic brain tomography (LORETA) were developed in order to identify brain regions involved in neuropsychiatric disorders. Since the progression of both neurological and cognitive impairment is slow, general categorization of EEG aberrations may not reach sufficient sensitivity for the detection and localization of abnormalities. EEG tomography allows a detection of dysfunction that is more sensitive than that provided by the common EEG. LORETA also offers new hypotheses on the location of higher cognitive functions in the brain [35]. Taken together, the advantages of LORETA over surface EEG analysis include the ability to visualize anomalies in the deeper brain structures and to specify anomalies in frequency band and spatial location. LORETA technique has also been used to compare with ICA method.

Finally, in order to evaluate the whole performance of the proposed RBF, a set of EEGs with all the types of noise was selected. The ICA systems were chosen as a function of their previous performance. Figure 7 plots the noise effect in a EEG segment. The result after applying the LORETA technique is observed on the right. It is difficult to know the lobe in which neuronal activity has been generated. As can be observed, the RBF system was able to remove the interference and allowed one to clearly appreciate the brain waves. Therefore, in Fig. 9 the neuronal activity can be analysed and located in temporal lobes. Besides in EEG signal, a low-frequency oscillation corresponding to alpha rhythms can be detected. On the contrary, the ICA system removed part of the noise, but clearly affected the original EEG signal waveform, thus distorting the final result and turning any other later analysis more difficult as shown in Fig. 8.

Table 4 Comparison of the MSE between RBF and other methods filtering baseline noise (average values \pm SD)

Frequency	0.1 Hz				0.2 Hz			
	SNR(dB)		-2	-5	1.2	-2	-5	-2
MSE	Wavelet	0.37 ± 0.09	0.44 ± 0.08	0.57 ± 0.09	0.45 ± 0.08	0.88 ± 0.09	5.89 ± 0.15	
SVD		0.26 ± 0.07	0.38 ± 0.07	0.49 ± 0.07	0.41 ± 0.07	0.82 ± 0.08	5.57 ± 0.13	
PCA		0.47 ± 0.08	0.59 ± 0.08	0.73 ± 0.08	0.56 ± 0.08	1.09 ± 0.08	5.96 ± 0.13	
AF		0.25 ± 0.06	0.39 ± 0.06	0.51 ± 0.06	0.45 ± 0.06	0.73 ± 0.07	4.93 ± 0.12	
HF		0.23 ± 0.06	0.35 ± 0.05	0.47 ± 0.05	0.29 ± 0.06	0.53 ± 0.07	4.72 ± 0.11	
ICA		0.22 ± 0.05	0.32 ± 0.05	0.43 ± 0.05	0.25 ± 0.05	0.41 ± 0.06	4.59 ± 0.09	
RBF		0.12 ± 0.04	0.27 ± 0.04	0.41 ± 0.03	0.22 ± 0.03	0.36 ± 0.05	0.78 ± 0.04	
Frequency	0.4 Hz				0.6 Hz			
	SNR(dB)		-2	-5	1.2	-2	-5	-2.7
MSE	Wavelet	8.71 ± 0.17	41 ± 1.92	175 ± 3.36	42 ± 1.65	78 ± 2.18	160 ± 4.45	
SVD		7.69 ± 0.15	38 ± 1.87	142 ± 3.26	39 ± 1.59	69 ± 2.09	141 ± 4.56	
PCA		9.32 ± 0.17	46 ± 1.95	173 ± 3.31	47 ± 1.63	79 ± 1.73	158 ± 4.38	
AF		7.52 ± 0.14	32 ± 1.23	119 ± 2.78	36 ± 1.34	63 ± 1.46	123 ± 4.02	
HF		6.87 ± 0.12	27 ± 1.15	108 ± 2.26	28 ± 1.22	57 ± 1.38	119 ± 3.71	
ICA		6.13 ± 0.10	22 ± 1.03	97 ± 1.87	23 ± 1.05	49 ± 1.27	113 ± 3.36	
RBF		0.32 ± 0.05	0.74 ± 0.06	0.93 ± 0.03	0.96 ± 0.05	1.91 ± 0.07	3.64 ± 0.12	

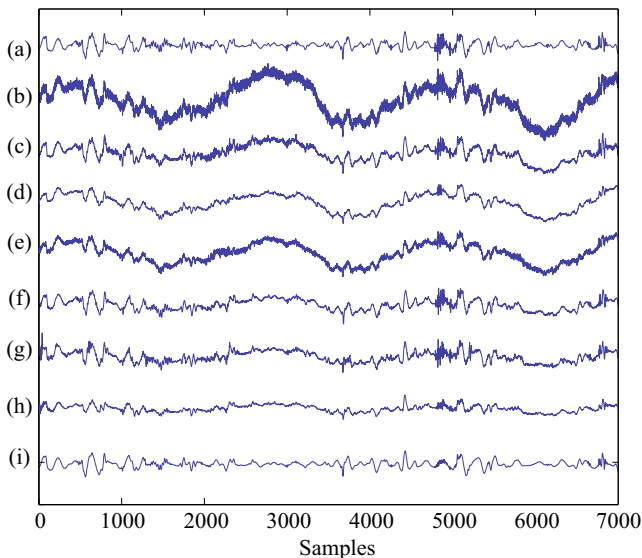


Fig. 6 Comparison of baseline noise removal by the proposed system and standard filtering techniques for Fp1-F7 derivation. *a* Original recording without processing. *b* Input signal of 8 dB baseline noise used to compare the different methods. *c* Filtering results for baseline noise with the wavelet method. *d* Filtering results for baseline noise with the SVD method. *e* Filtering results for baseline noise with the PCA method. *f* Filtering results for baseline noise with the AF method. *g* Filtering results for baseline noise with the HF method. *h* Filtering results for baseline noise with the ICA method. *i* Filtering results for baseline noise with the RBF

5 Discussion

In this study, a new RBF model to reduce different types of noise in EEG signals has been proposed. Noise reduction and cancellation are important for obtaining a clear and useful signal. Some signals, such as EEG, are non-stationary, and the noise statistical property is complicated because of the complexity of the signal.

During last years, numerous techniques have been proposed to reject different kinds of noise in EEG signals, including wavelet, SVD, PCA, AF, HF and ICA. However, optimized results have not yet been obtained. In addition, these conventional filtering techniques can contain ripples that do not correspond to the original EEG. We have found that RBF improves all results obtained by the previous methods significantly reducing the interference. Moreover, SNRI evolution has been more constant with RBF and more linear because the proposed method has introduced the lowest distortion to the signal. With baseline noise, RBF has achieved higher SIR and CC values and a smaller MSE than the other methods, reducing the noise and correcting the variation produced by the baseline noise.

Taken together, the presented results demonstrate that the proposed ANN approach can serve as a new framework for achieving an efficiently filtered ECG signal which, obviously, could be used for later studies in the best conditions [46]. Another relevant issue is properly studying the filtering procedure. Though traditional filtering techniques can be used as tools for noise removal from the ECG, over-filtering signals

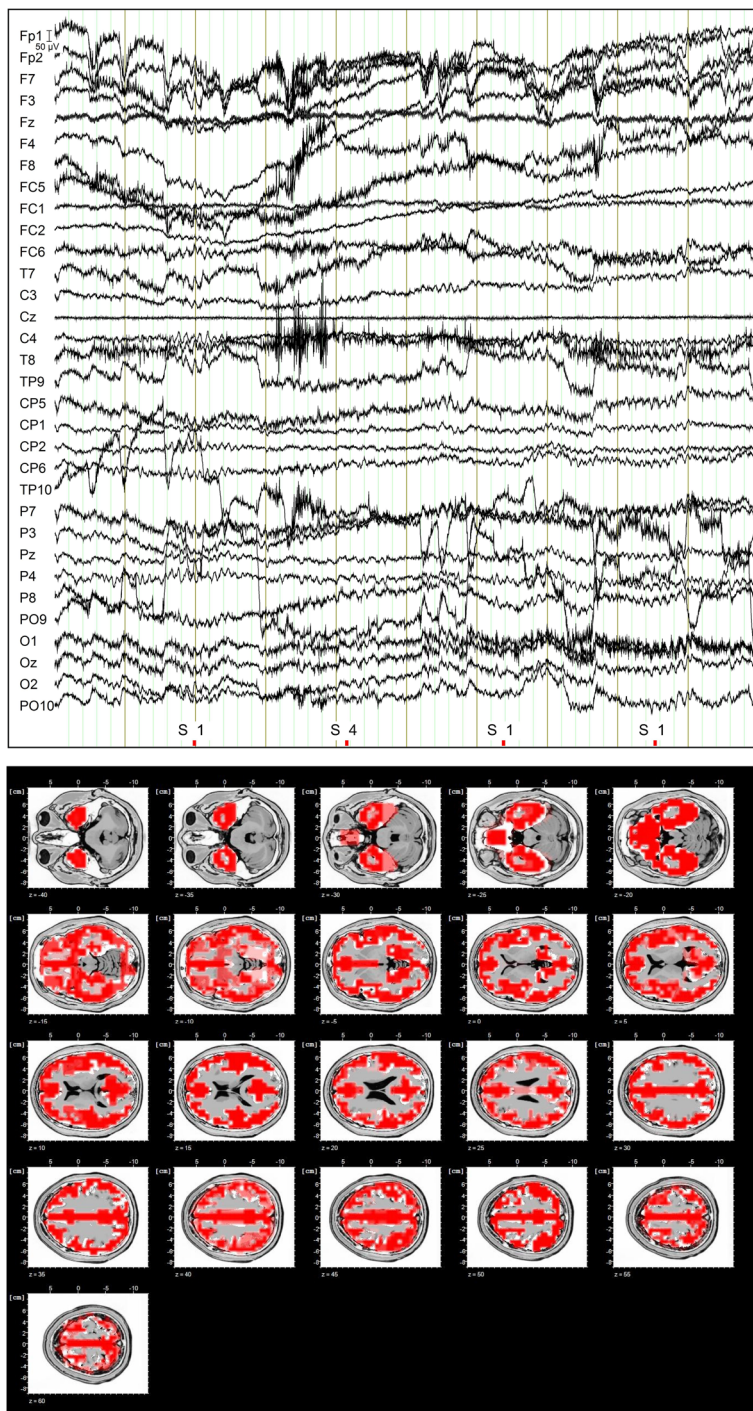


Fig. 7 Raw EEG segments with muscle and baseline noise and LORETA maps

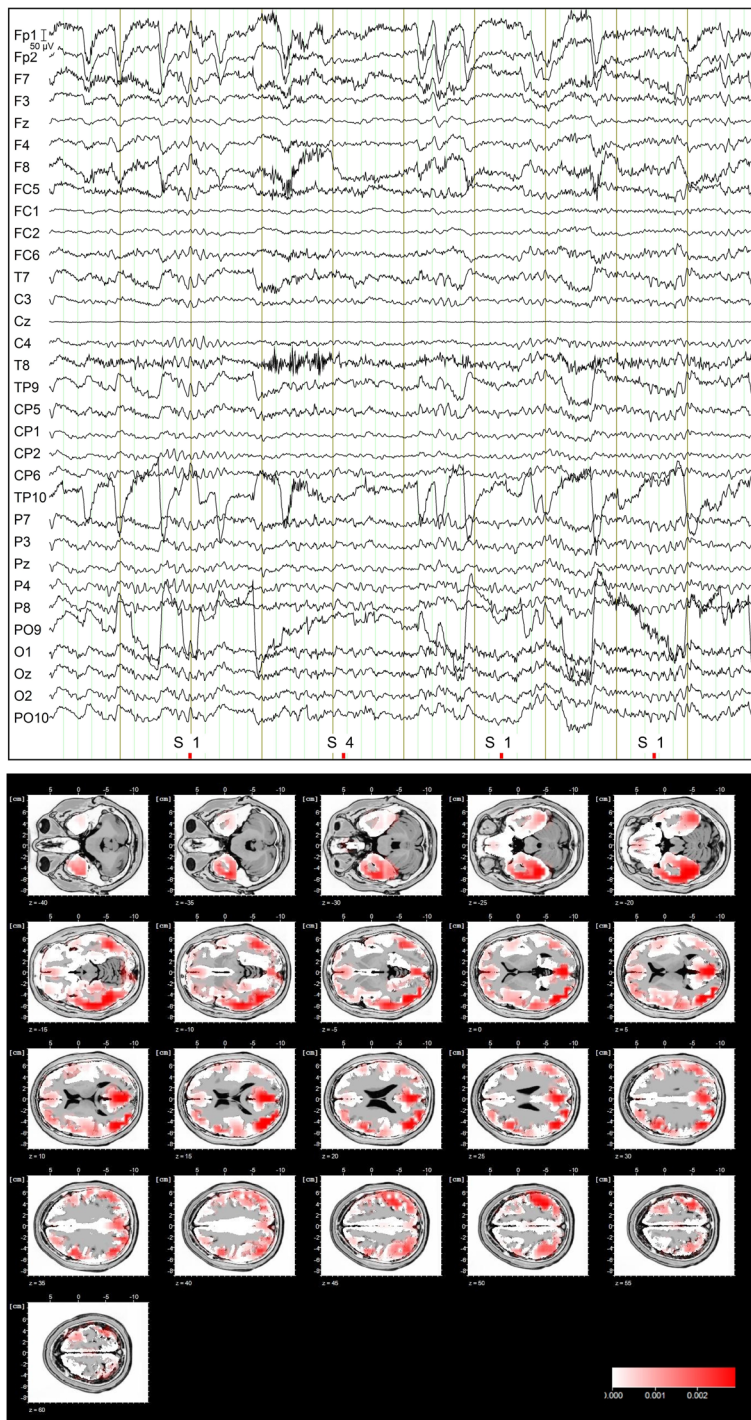


Fig. 8 EEG signals corrected for noise by means of ICA method and LORETA maps

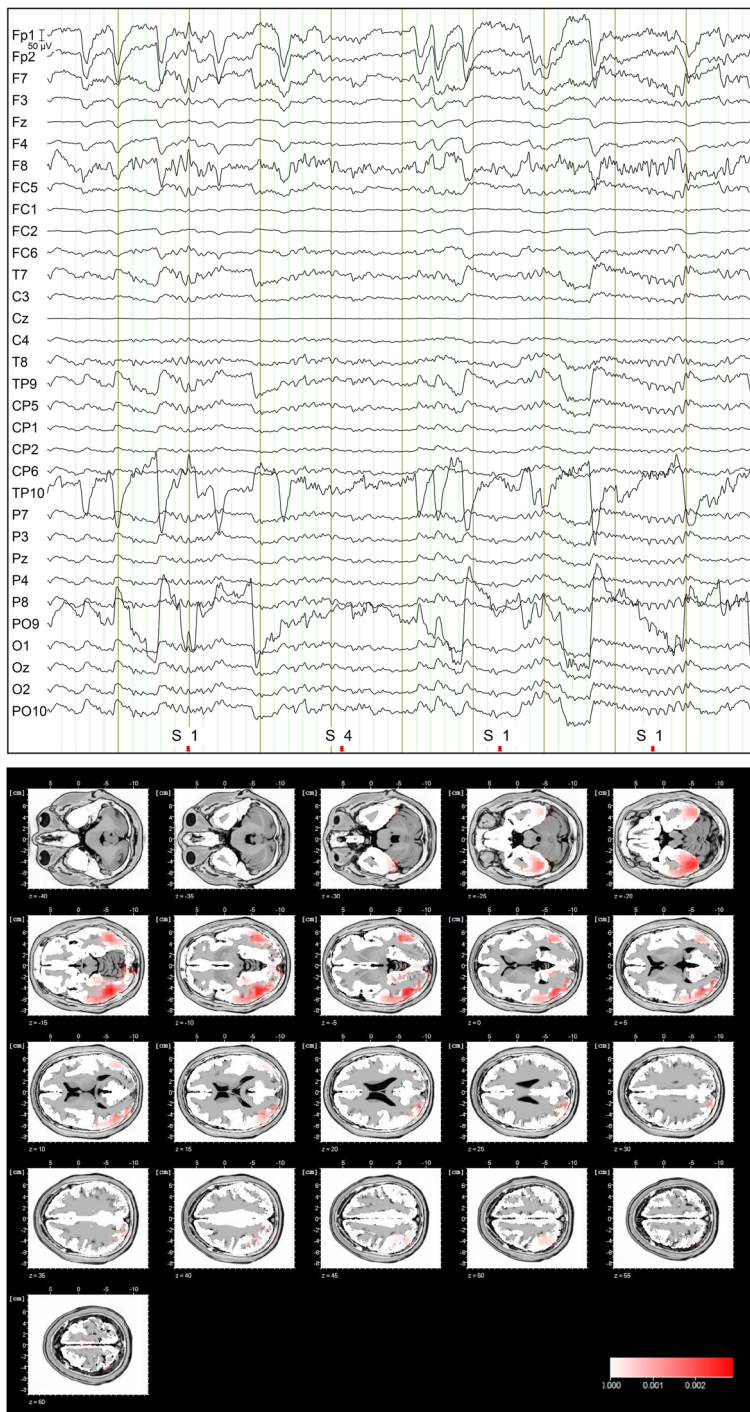


Fig. 9 EEG signals corrected for noise by means of RBF method and LORETA maps

can remove or distort relevant clinical information. On the contrary, the results of this study suggest that clinical information can be maintained by selecting a flexible dynamic model for the ECG and an adaptive update of the model parameters.

6 Conclusion

The present study has demonstrated how the proposed RBF can be used to reduce muscle and baseline noise in EEG recordings in one step. Throughout all stages, the RBF method has been adapted using the SP method, which has been improved to achieve our target. RBF has obtained greater CC and SIR values than the other methods and a more stable SNRI value. Besides, this method has revealed to be an effective enhancement tool in all practical cases which have been studied, keeping clinical information in the brain signal. As a way of conclusion, suffice is to say that the RBF-based approach has obtained both more signal reduction and low distortion of the signal results in comparison with systems based on wavelet, SVD, PCA, AF, HF and ICA methods. The technique proposed through this paper finds its application by means of denoising biological signals.

Acknowledgments This work was sponsored by the Castilla-La Mancha Research Scheme (PPII-2014-024-P), the University of Castilla-La Mancha and the Virgen de la Luz Hospital of Cuenca (Spain).

References

1. M.T. Akhtar, W. Mitsuhashi, C.J. James, Employing spatially constrained ICA and wavelet denoising, for automatic removal of artifacts from multichannel EEG data. *Signal Process.* **92**(2), 401–416 (2012)
2. E. Alickovic, A. Subasi, Effect of multiscale pca de-noising in ecg beat classification for diagnosis of cardiovascular diseases. *Circuits Syst. Signal Process.* **34**, 513–533 (2015)
3. U. Aydin, Y.S. Dogrusoz, A kalman filter-based approach to reduce the effects of geometric errors and the measurement noise in the inverse ecg problem. *Med. Biol. Eng. Comput.* **49**(9), 1003–1013 (2011)
4. C.M. Bishop, *Neural Networks for Pattern Recognition* (Oxford Univ Press, New York, 1995)
5. L. Bor-Shyh, S. Ming-Jen, C. Ching-Chin, T. Kuan-Chih, C. Jen-Yin, Enhancing bowel sounds by using a higher order statistics-based radial basis function network. *IEEE Biomed. Health Inform.* **17**(3), 675–680 (2013)
6. L. Boubchir, B. Boashash, Wavelet denoising based on the map estimation using the BKF prior with application to images and EEG signals. *IEEE Trans. Signal Process.* **61**(8), 1880–1894 (2013)
7. S. Boudet, L. Peyrodié, G. Forzy, A. Pinti, H. Toumi, P. Gallois, Improvements of adaptive filtering by optimal projection to filter different artifact types on long duration eeg recordings. *Comput. Methods Progr. Biomed.* **108**(1), 234–249 (2012)
8. M.D. Buhmann, *Radial Basis Functions. Theory and Implementations* (Cambridge University Press, Cambridge, 2003)
9. E. Castillo, D.P. Morales, G. Botella, A. Garca, L. Parrilla, A.J. Palma, Efficient wavelet-based ECG processing for single-lead FHR extraction. *Digit. Signal Proc.* **23**(6), 1897–1909 (2013)
10. M.P.S. Chawla, A comparative analysis of principal component and independent component techniques for electrocardiograms. *Neural Comput. Appl.* **18**(6), 539–556 (2009)
11. M.P.S. Chawla, PCA and ICA processing methods for removal of artifacts and noise in electrocardiograms: a survey and comparison. *Appl. Soft Comput.* **11**(2), 2216–2226 (2011)
12. W. Dong-Qing, L. Hua-Bo, D. Feng, Highly efficient identification methods for dual-rate Hammerstein systems. *IEEE Trans. Control Syst. Technol.* **23**(5), 1952–1960 (2015)
13. M. Fatourechi, A. Bashashati, R.K. Ward, G.E. Birch, EMG and EOG artifacts in brain computer interface systems: a survey. *Clin. Neurophysiol.* **118**, 480–494 (2007)
14. D. Grupe, *Principles of Artificial Neural Networks*, 2nd edn. (World Scientific, River Edge, 2007)

15. J.T. Gwin, K. Gramann, S. Makeig, D.P. Ferris, Removal of movement artifact from high-density eeg recorded during walking and running. *J. Neurophysiol.* **103**(6), 3526–3534 (2010)
16. S. Haykin, *Adaptive Filter Theory*, 2nd edn. (Prentice-Hall, Englewood Cliffs, 1991)
17. S. Haykin, *Neural Networks: A Comprehensive Approach*, 2nd edn. (Prentice-Hall, Upper Saddle River, 1999)
18. S. Haykin, *Neural Networks and Learning Machines*, 3rd edn. (Prentice Hall, Upper Saddle River, 2008)
19. J. Jeraj, V.J. Mathews, A stable adaptive Hammerstein filter employing partial orthogonalization of the input signals. *IEEE Trans. Signal Process.* **54**(4), 1412–1420 (2006)
20. N.B. Karayiannis, M.M. Randolph-Gips, Self-organizing radial basis function network for real-time approximation of continuous-time dynamical systems. *IEEE Trans. Neural Netw.* **19**(3), 460–474 (2008)
21. T. Kathirvalavakumar, *Neural Networks: FNN Training Algorithms: Simultaneous perturbation, Back-propagation and Tunneling Methods* (VDM Verlag, Saarbrücken, 2010)
22. T.D. Lagerlund, F.W. Sharbrough, N.E. Busacker, Use of principal component analysis in the frequency domain for mapping electroencephalographic activities: comparison with phase-encoded fourier spectral analysis. *Brain Topogr.* **17**(2), 73–84 (2004)
23. V. Lan-Da, W. Di-You, C. Chien-Shiun, Energy-efficient fastica implementation for biomedical signal separation. *IEEE Trans. Neural Netw.* **22**(11), 1809–1822 (2011)
24. J.A. Leonard, M.A. Kramer, L.H. Ungar, Using radial basis functions to approximate a function and its error bounds. *IEEE Trans. Neural Netw.* **3**(4), 624–627 (1992)
25. K. Li, M.N.S. Swamy, M.O. Ahmad, An improved voice activity detection using higher order statistics. *IEEE Trans. Speech Audio Process.* **13**(5), 965–974 (2005)
26. W. Li, H. Yang, A non-linear blind source separation method based on perceptron structure and conjugate gradient algorithm. *Circuits Syst. Signal Process.* **33**, 3573–3590 (2014)
27. B.S. Lin, B.S. Lin, F.C. Chong, F. Lai, Higher-order-statistics-based radial basis function networks for signal enhancement. *IEEE Trans. Neural Netw.* **18**(3), 823–832 (2007)
28. Z. Liu, J.A. de Zwart, P. van Gelderen, L.-W. Kuo, J.H. Duyn, Statistical feature extraction for artifact removal from concurrent fMRI-EEG recordings. *NeuroImage* **59**(3), 2073–2087 (2012)
29. S. Lo-Chyuan, J. Yue-Dar, C. Fu-Kun, S. Chao-Ming, Neural network-based IIR all-pass filter design. *Circuits Syst. Signal Process.* **33**, 437–457 (2014)
30. S. Luo, P. Johnston, A review of electrocardiogram filtering. *J. Electrocardiol.* **43**(6), 486–496 (2010)
31. J. Ma, P. Tao, S. Bayram, V. Svetnik, Muscle artifacts in multichannel eeg: characteristics and reduction. *Clin. Neurophysiol.* **123**(8), 1676–1686 (2012)
32. J. Mateo, A.M. Torres, E.M. Sánchez-Morla, J.L. Santos, Eye movement artefact suppression using Volterra filter for electroencephalography signals. *J. Med. Biol. Eng.* **35**(3), 395–405 (2015)
33. J. Mateo, A.M. Torres, A. Aparicio, J.L. Santos, An efficient method for ECG beat classification and correction of ectopic beats. *Comput. Electr. Eng.*, 1–11 (2016). doi:[10.1016/j.compeleceng.2015.12.015](https://doi.org/10.1016/j.compeleceng.2015.12.015)
34. C.L. Nikias, A.P. Petropulu, *Higher-Order Spectra Analysis: A Nonlinear Signal Processing Framework* (Prentice-Hall, Englewood Cliffs, 1993)
35. R.D. Pascual-Marqui, M. Esslen, K. Kochi, D. Lehmann, Functional imaging with low resolution brain electromagnetic tomography (LORETA): a review. *Methods Find. Exp. Clin. Pharmacol.* **24**C, 91–95 (2002)
36. J.S. Paul, M.R. Reddy, V.J. Kumar, A transform domain SVD filter for suppression of muscle noise artefacts in exercise ECG's. *IEEE Trans. Biomed. Eng.* **47**(5), 654–663 (2000)
37. G. Peccati, *Wiener Chaos: Moments, Cumulants and Diagrams: A survey with Computer Implementation* (Springer, Milano, 2011)
38. R. Romo, Vázquez, H. Vélez-Pérez, R. Ranta, V. Louis Dorr, D. Maquin, L. Maillard, Blind source separation, wavelet denoising and discriminant analysis for EEG artefacts and noise cancelling. *Biomed. Signal Process. Control* **7**(4), 389–400 (2012)
39. R. Sameni, M.B. Shamsollahi, C. Jutten, Model-based bayesian filtering of cardiac contaminants from biomedical recordings. *Physiol. Meas.* **29**(5), 595–613 (2008)
40. R. Sameni, M.B. Shamsollahi, C. Jutten, G.D. Clifford, A nonlinear bayesian filtering framework for ECG denoising. *IEEE Trans. Biomed. Eng.* **54**(12), 2172–2185 (2007)
41. M. Sansone, L. Mirarchi, M. Bracale, Adaptive removal of gradients-induced artefacts on ECG in MRI: a performance analysis of RLS filtering. *Med. Biol. Eng. Comput.* **48**(5), 475–482 (2010)

42. R.J. Schilling, J.J. Carroll, A.F. Al-Ajlouni, Approximation of nonlinear systems with radial basis function neural network. *IEEE Trans. Neural Netw.* **12**(1), 1–15 (2001)
43. R. Shanmugam, R. Chattamvelli, *Statistics for Scientists and Engineers* (Wiley, New York, 2015)
44. S.Y. Shao, K.Q. Shen, C.J. Ong, E.P.V. Wilder-Smith, X.P. Li, Automatic eeg artifact removal: a weighted support vector machine approach with error correction. *IEEE Trans. Biomed. Eng.* **56**(2), 336–344 (2009)
45. L.N. Sharma, S. Dandapat, A. Mahanta, ECG signal denoising using higher order statistics in wavelet subbands. *Biomed. Signal Process. Control* **5**(3), 214–222 (2010)
46. L. Sörnmo, P. Laguna, *Bioelectrical Signal Processing in Cardiac and Neurological Applications* (Elsevier Academic Press, Amsterdam, 2005)
47. E.M. ter Braack, B. de Jonge, M.J.A.M. van Putten, Reduction of TMS induced artifacts in EEG using principal component analysis. *IEEE Trans. Neural Syst. Rehabil. Eng.* **21**(3), 376–382 (2013)
48. A.M. Torres, J. Mateo, M.A. García, J.L. Santos, Cancellation of powerline interference from biomedical signals using an improved affine projection algorithm. *Circuits Syst. Signal Process.* **34**(4), 1249–1264 (2015)
49. R. Vullings, B. de Vries, J. Bergmans, An adaptive kalman filter for ECG signal enhancement. *IEEE Trans. Biomed. Eng.* **58**(4), 1094–1103 (2011)
50. T.J. Willink, Efficient adaptive SVD algorithm for MIMO applications. *IEEE Trans. Signal Process.* **56**(2), 615–622 (2008)
51. Y. Wu, R.M. Rangayyan, Y. Zhouc, S.C. Ngd, Filtering electrocardiographic signals using an unbiased and normalized adaptive noise reduction system. *Med. Eng. Phys.* **31**(1), 17–26 (2009)
52. H. Yang, S.T. Bukkanpatnam, R. Komanduri, Nonlinear adaptive wavelet analysis of electrocardiogram signals. *Phys. Rev.* **76**(2), 026214 (2007)
53. Q. Yi, L. Zhan-Ming, L. Er-Chao, Fault tolerant control for non-gaussian stochastic distribution systems. *Circuits Syst. Signal Process.* **32**, 361–373 (2013)
54. L. Yu, S. Fei, J. Huang, Y. Gao, Trajectory switching control of robotic manipulators based on rbf neural networks. *Circuits Syst. Signal Process.* **33**, 1119–1133 (2014)